

## Electronic structures and optical properties of short-period GaAs/AlAs superlattices

Jian-Bai Xia\* and Yia-Chung Chang

*Department of Physics and Materials Research Laboratory, University of Illinois at Urbana-Champaign,  
1110 West Green Street, Urbana, Illinois 61801*

(Received 10 January 1990)

Electronic and optical properties of short-period superlattices are investigated with an empirical tight-binding model, which includes second-neighbor interactions. The  $\Gamma$ - and  $X$ -like electronic energy levels are obtained as functions of the number of GaAs monolayers, the applied electric field, and the parallel wave vector. The calculated  $\Gamma$ - $X$  crossover is in good agreement with the experimental observation. Short-period superlattices grown in the [111] direction are also examined. Dielectric functions of superlattices over the full energy range are calculated by using a newly developed empirical method to obtain optical matrix elements. Dielectric functions of short-period superlattices are found to be quite different from those of bulk GaAs and AlAs, but fairly close to their average when the number of monolayers of GaAs and AlAs in the superlattice are the same and larger than six.

### I. INTRODUCTION

Electronic structures of short-period GaAs/AlAs superlattices (SL's) have been investigated widely in both experimental and theoretical aspects.<sup>1-19</sup> One of the most interesting questions in short-period superlattices is the crossover of the direct and indirect transitions. Finkman *et al.*<sup>1</sup> first found a long-lived emission labeled  $X_{xy}$  at low temperatures in AlAs/GaAs superlattices, which is associated with an  $X$  electron in AlAs and a  $\Gamma$  hole in GaAs. The peak of the excitation spectrum  $\Gamma_H$ , involving a heavy hole and a  $\Gamma$  electron in GaAs, is higher than the  $X_{xy}$  peak when the thickness of GaAs is smaller than 29 Å. Nagle *et al.*<sup>2</sup> and Moore *et al.*<sup>3</sup> also reported similar results. Danan *et al.*<sup>4</sup> studied photoluminescence (PL) of direct- and indirect-gap GaAs/AlAs superlattices under an electric field perpendicular to the layers, and found that in the direct-transition case the quantum-confined Stark effect is observed. In the indirect-transition case reverse Stark shifts are found, providing evidence that  $X$ -like electronic states are confined in the AlAs layers. Meynadier *et al.*<sup>5</sup> demonstrated that a GaAs/AlAs superlattice (35 Å/80 Å) can be switched from indirect to direct, in both real and reciprocal spaces, by the application of a modest axial electric field. An anticrossing behavior was found, manifesting the presence of  $\Gamma$ - $X$  mixing by a potential term measured to be of the order of 1-3 meV. Recent spectroscopic investigations<sup>6,7</sup> estimated the crossover of the direct and indirect transitions to occur at a number of GaAs monolayers ( $M$ ) near 11, but there was also spectroscopic measurement,<sup>8</sup> predicting the crossover to occur at  $M=7$ .

Early theoretical results<sup>9-12</sup> about the crossover of the  $\Gamma$ - and  $X$ -like levels are controversial. Recently, Gell *et al.*<sup>13</sup> and Xia<sup>14</sup> calculated the electronic structures of short-period superlattices with empirical pseudopotential methods. They predicted that the crossover occurs at  $M=8$  and  $M>10$ , respectively. Ihm<sup>15</sup> calculated the

GaAs/AlAs superlattice with a nearest-neighbor tight-binding model and demonstrated that if the thickness of the GaAs layer is less than 30 Å, the lowest conduction-band state is  $X$ -like, confined to the AlAs barrier region. Because the nearest-neighbor tight-binding model predicts artificially dispersionless bulk bands for wave vectors at  $(1,0,\xi)(2\pi/a)$  with  $\xi$  going from 0 to 1, the GaAs and AlAs layers are completely decoupled for the  $X_{xy}$  state. Thus, the energy of the lowest  $X_{xy}$  conduction state of the superlattice is identical to that of the bulk AlAs  $X$  state. This decoupling would lead to wrong ordering of the superlattice  $X_{xy}$  and  $X_z$  states. Brey *et al.*<sup>16</sup> used a similar nearest-neighbor tight-binding model and discovered that the lowest  $\Gamma$ - and  $X$ -like states cross at  $M=18$  for  $(\text{GaAs})_M(\text{AlAs})_{18}$  superlattices. Lu and Sham<sup>17</sup> and Fujimoto *et al.*<sup>18</sup> performed energy-band calculations using an empirical tight-binding model which includes the second-neighbor interactions. Fujimoto *et al.* found that the lowest transition is forbidden for superlattices with  $M$  less than 5. Lu and Sham put emphasis on the effect of valley mixing. The same effect was first predicted by Ting and Chang<sup>19</sup> within a one-band Wannier model. The Wannier model predicts that the  $\Gamma$ - $X$  mixing occurs only at an odd number of AlAs monolayers,<sup>19</sup> while the tight-binding model of Lu and Sham predicts it to occur only at an even number of AlAs monolayers. We shall show that such a prediction is sensitive to the choice of the tight-binding parameters. For the tight-binding model used in the present paper, we predict the same behavior as that of the Wannier model.

In the first part of this paper we calculate the electronic structures of short-period superlattices with an empirical tight-binding model that includes second-neighbor interactions. The second-neighbor interactions are essential for obtaining the correct ordering of superlattice energy bands derived from various  $X$  valleys. Our theoretical predictions are compared with recent experimental results.

Many applications of GaAs and related superlattices depend on the dielectric function  $\epsilon(\omega)$ , which is related to the energy-band structure and optical transition matrix elements between states of valence and conduction bands. There are many experimental<sup>20</sup> and theoretical<sup>21–23</sup> investigations in the dielectric functions of GaAs and other III-V semiconducting compounds, but there are few experimental investigations on the dielectric functions of superlattices.<sup>24,25</sup> Previous theoretical investigations are only limited to the energy range near the direct band gap.<sup>26,27</sup> In the second part of this paper we calculate the dielectric functions of bulk GaAs and GaAs/AlAs short-period superlattices within the framework of the tight-binding model. For calculating the dielectric function of superlattices in the full energy range, we use the method developed in Refs. 28 and 29 to determine the optical matrix elements between atomic orbitals of the same and nearest-neighbor atoms by fitting the squared optical matrix elements of bulk GaAs over the whole Brillouin zone, with corresponding matrix elements calculated with the empirical pseudopotential method.

## II. THEORETICAL METHOD AND ITS APPLICATION TO BULK MATERIALS

In this paper we use a second-neighbor tight-binding model with four orbitals ( $sp^3$ ) per atom. There are 19 empirical parameters for each III-V semiconducting compound to describe the interactions:  $E_s^a, E_p^a, E_s^c, E_p^c, V_{ss}, V_{sp1}, V_{s1p}, V_{xx}, V_{xy}, E_{ss}^a, E_{sx}^a, E_{xx}^a, E_{xy}^a, E_{zz}^a, E_{ss}^c, E_{sx}^c, E_{xx}^c, E_{xy}^c,$  and  $E_{zz}^c$ . The first four are the on-site orbital energies with superscripts  $a$  and  $c$  standing for anion and cation, respectively. The fifth to ninth are the nearest-neighbor interaction parameters as defined in Ref. 30. The last ten are second-neighbor interaction parameters between two anion or cation orbitals, one centered at the origin and the other centered at  $\mathbf{R}_{110} = (1, 1, 0)(a/2)$ . For example,

$$E_{\alpha\alpha'}^a = \langle \phi_\alpha^a(\mathbf{0}) | H | \phi_{\alpha'}^a(\mathbf{R}_{110}) \rangle, \quad (1)$$

where  $\phi_\alpha^a(\mathbf{R})$  denotes an  $\alpha$ -like anion atomic orbital centered at  $\mathbf{R}$ . Here we have not used the two-center approximation; hence  $E_{zz}^a \neq E_{xx}^a - E_{xy}^a$ . The relaxation of the two-center approximation is essential for obtaining

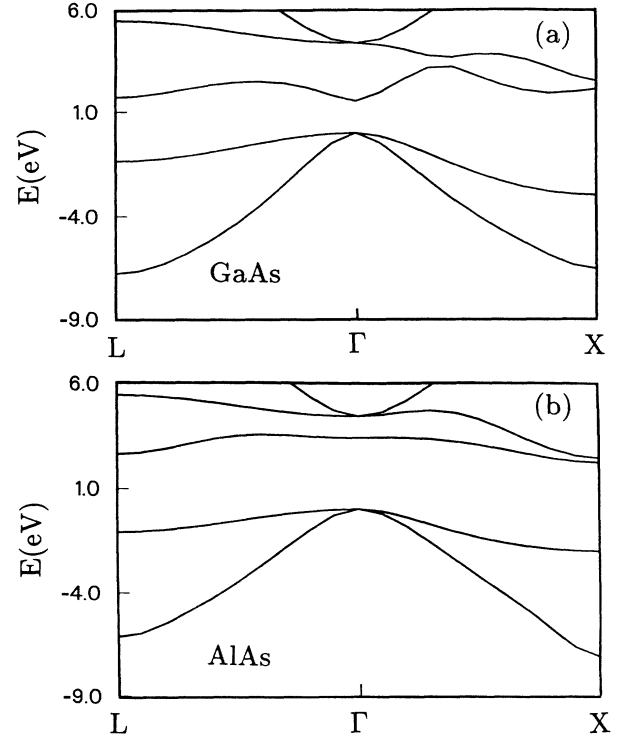


FIG. 1. Band structures of (a) GaAs and (b) AlAs obtained with the present tight-binding model.

good overall conduction-band structures.

The 19 parameters are determined by fitting the energy bands calculated by the tight-binding method with the corresponding results obtained by an empirical pseudopotential method (EPM) with special emphasis on the conduction bands. The optimized parameters are shown in Table I. The band structures of bulk GaAs and AlAs calculated with these parameters are shown in Fig. 1. The energies at  $\Gamma$ ,  $X$ , and  $L$  points are given in Table II. From Fig. 1 and Table II we see that the valence bands (except the lowest one) as well as the four conduction bands are in good agreement with the EPM results.

TABLE I. Interaction parameters in the second-neighbor tight-binding model, in eV.

| Material | $E_s^a$    | $E_p^a$    | $E_s^c$    | $E_p^c$    | $V_{ss}$   | $V_{xx}$   |
|----------|------------|------------|------------|------------|------------|------------|
| GaAs     | -8.9795    | 0.7303     | -4.3878    | 3.2195     | -9.8302    | 0.4189     |
| AlAs     | -9.2592    | 1.3773     | -4.2975    | 3.3108     | -11.7504   | 0.2314     |
|          | $V_{xy}$   | $V_{sp1}$  | $V_{s1p}$  | $E_{ss}^a$ | $E_{sx}^a$ | $E_{xx}^a$ |
|          | 5.9883     | 6.4075     | 4.0130     | -0.2094    | -0.3108    | 0.0327     |
|          | 5.9575     | 5.7316     | 4.3963     | -0.2628    | -0.2217    | 0.0593     |
|          | $E_{zz}^a$ | $E_{ss}^c$ | $E_{sx}^c$ | $E_{xx}^c$ | $E_{xy}^c$ | $E_{zz}^c$ |
|          | -0.2379    | -0.1244    | 0.2766     | 0.3507     | 0.0112     | -0.4143    |
|          | -0.4599    | -0.0860    | 0.4268     | 0.3194     | -0.0094    | -0.3609    |

TABLE II. Conduction-band energies at  $\Gamma, X, L$  points for GaAs and AlAs (in eV, relative to the top of the valence band).

| Material | $\Gamma$ | $X$    | $L$    |
|----------|----------|--------|--------|
| GaAs     | 1.5362   | 2.1730 | 1.6980 |
| AlAs     | 3.4014   | 2.2028 | 2.6389 |

The optical matrix elements between an atomic orbital of symmetry type  $\alpha$ , located at the origin and another atomic orbital of symmetry type  $\alpha'$ , located at position  $\tau$ , can be written as

$$P_{\alpha\alpha'}^\beta(\tau) = \frac{\hbar}{i} \left( \frac{2}{m} \right)^{1/2} \int \phi_\alpha(\mathbf{r}) \frac{\partial}{\partial \beta} \phi_{\alpha'}(\mathbf{r}-\tau) d^3r, \quad (2)$$

where  $\alpha, \alpha' = s, x, y, z$ , and  $\beta = x, y, z$  denotes the direction of polarization of the incident photon. The following relations were derived in Ref. 29, for anions and cations, respectively,

$$P_{s\beta}^\beta(0) = \begin{cases} iP_{aa'} \\ iP_{cc} \end{cases}. \quad (3)$$

For an anion located at origin and a cation located at  $\tau$ ,

$$\begin{aligned} P_{ss}^\beta(\tau) &= iP_{ss}\tau_\beta, \\ P_{as}^\beta(\tau) &= i[P_{ps}\tau_{\alpha'}\tau_\beta + P_{ps\pi}(\tau^2\hat{\beta}\cdot\hat{\alpha}' - \tau_\beta\tau_{\alpha'})], \\ P_{s\alpha'}^\beta(\tau) &= i[P_{sp}\tau_{\alpha'}\tau_\beta + P_{sp\pi}(\tau^2\hat{\beta}\cdot\hat{\alpha}' - \tau_\beta\tau_{\alpha'})], \\ P_{\alpha\alpha'}^\beta(\tau) &= i[P_{pp} - 3P_{pp\pi}(1 - \delta_{\alpha\alpha'} - \delta_{\beta\alpha'} - \delta_{\beta\alpha})]\tau_{\alpha'}\tau_\beta\tau_{\alpha'}, \end{aligned} \quad (4)$$

where  $\tau_\beta = \tau \cdot \hat{\beta}$ ,  $\tau_\alpha = \tau \cdot \hat{\alpha}$ ,  $\tau_{\alpha'} = \tau \cdot \hat{\alpha}'$ .  $P_{aa}, P_{cc}, P_{ss}, P_{ps}, P_{sp}, P_{pp}, P_{sp\pi}, P_{ps\pi}$ , and  $P_{pp\pi}$  are the empirical optical matrix parameters which can be determined by calculating the optical matrix elements between bulk valence- and conduction-band states over the entire Brillouin zone and fitting them to the corresponding EPM results. The optimum parameters are listed in Table III, and the comparison of the tight-binding fit with the EPM results for squared optical matrix elements of GaAs is shown in Fig. 2. For simplicity, we assume that the optical parameters for AlAs are the same as those for GaAs.

With the parameters given in Table III, we calculate the real part,  $\epsilon_1(\omega)$ , and imaginary part,  $\epsilon_2(\omega)$ , of the dielectric function of GaAs. They are given by

$$\epsilon_1(\hbar\omega) = 1 + \frac{8\pi e^2 \hbar^2}{mV} \sum_{\mathbf{k}, i, j} \frac{|\langle \mathbf{k}, i | P_\beta | \mathbf{k}, j \rangle|^2}{(E_j - E_i)[(E_j - E_i)^2 - \hbar^2\omega^2]}, \quad (5)$$

$$\epsilon_2(\hbar\omega) = \frac{4\pi^2 e^2}{mV\omega^2} \sum_{\mathbf{k}, i, j} |\langle \mathbf{k}, i | P_\beta | \mathbf{k}, j \rangle|^2 \delta(E_j - E_i - \hbar\omega), \quad (6)$$

where

$$P_\beta = \frac{\hbar}{i} \left( \frac{2}{m} \right)^{1/2} \frac{\partial}{\partial \beta}. \quad (7)$$

$\epsilon_1(\hbar\omega)$  can be calculated from  $\epsilon_2(\hbar\omega)$  by use of the Kramers-Kronig relation; it can also be calculated directly from Eq. (5). In order to obtain a smooth  $\epsilon(\hbar\omega)$ , we replace the  $\delta$  function in Eq. (6) by a Lorentzian function with a half-width  $\Gamma$ ,

$$\delta(E_j - E_i - \hbar\omega) \approx \frac{\Gamma/\pi}{(E_j - E_i - \hbar\omega)^2 + \Gamma^2}, \quad (8)$$

and in Eq. (5),

$$\frac{1}{E_j - E_i - \hbar\omega} \approx \frac{E_j - E_i - \hbar\omega}{(E_j - E_i - \hbar\omega)^2 + \Gamma^2}. \quad (9)$$

We use special points in the Brillouin zone<sup>31</sup> to calculate the summation in Eqs. (5) and (6), and gradually increase the density of special points until the results converge. We found that the results with 408 special points in the  $\frac{1}{48}$  Brillouin zone  $[(\frac{1}{32}, \frac{1}{32}, \frac{1}{32}), \dots]$  are nearly the same as those calculated with 2992 special points  $[(\frac{1}{64}, \frac{1}{64}, \frac{1}{64}), \dots]$ , and basically independent of the half-width  $\Gamma$ .

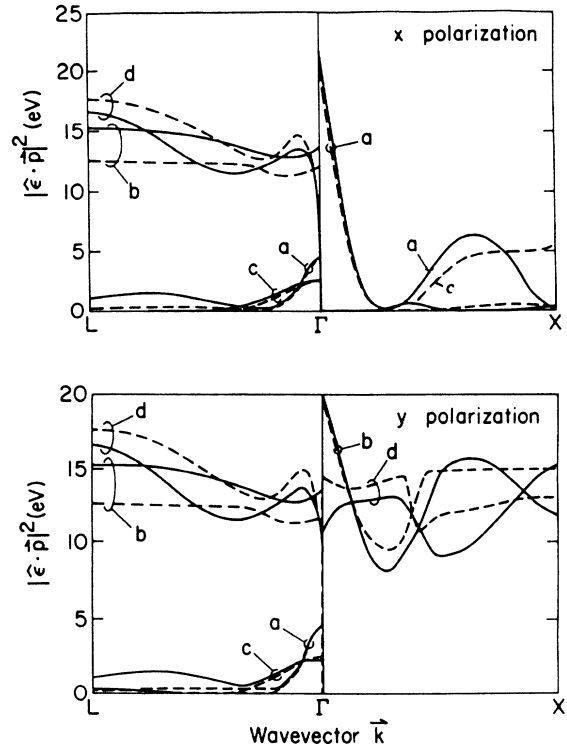


FIG. 2. Squared optical matrix elements  $|\hat{\epsilon} \cdot \mathbf{P}|^2$  of GaAs as functions of the wave vector ( $\mathbf{k}$ ) along the  $[110]$  ( $\Gamma$ - $X$ ) and  $[111]$  ( $\Gamma$ - $L$ ) directions. Solid and dashed curves are obtained by the present tight-binding model and the empirical pseudopotential model, respectively. *a*: transitions from the light-hole band to the first conduction band. *b*: transitions from the heavy-hole band to the first conduction band. *c*: transitions from the light-hole band to the second conduction band. *d*: transitions from the heavy-hole band to the second conduction band.

TABLE III. Parameters for GaAs optical matrix elements in  $\text{eV}^{1/2}$ .

| $P_{aa}$    | $P_{sp}$    | $P_{ps}$    | $P_{cc}$ | $P_{ss}$  | $P_{pp}$  |
|-------------|-------------|-------------|----------|-----------|-----------|
| 5.128 39    | 0.272 90    | 0.285 60    | 1.795 00 | -1.498 49 | -1.109 70 |
| $P_{sp\pi}$ | $P_{ps\pi}$ | $P_{pp\pi}$ |          |           |           |
| -0.578 37   | 0.000 18    | -0.071 64   |          |           |           |

The calculated  $\epsilon_1(E)$  and  $\epsilon_2(E)$  of GaAs and AlAs are shown in Fig. 3. The calculated  $\epsilon_1(E)$  and  $\epsilon_2(E)$  of GaAs and AlAs are in good agreement with experimental results<sup>20,32</sup> with differences which can be explained by the excitonic and local-field effects.<sup>33</sup> The good agreement between theory and experiment indicates that it is a fair approximation to use GaAs optical parameters for AlAs. We also calculate the contributions from various regions around  $\Gamma$ ,  $X$ ,  $L$ , and  $K$  points in the Brillouin zone to  $\epsilon_1(E)$  and  $\epsilon_2(E)$ , so that we can identify the origins of peaks in the  $\epsilon_1(E)$  and  $\epsilon_2(E)$  curves. For example, the peaks marked  $E_1$  and  $E_2$  are derived from regions near  $L$  and  $X$ , respectively. Our identifications agree with Refs.

20 and 32.

It is straightforward to apply the above tight-binding model to superlattices. At the interface the band parameters  $E_s^a, E_p^a$  for the interface atom As and  $E_s^c, E_{sx}^c, E_{xx}^c, E_{xy}^c, E_{zz}^c$  for cations Ga and Al at the two sides of the interface are taken as averages of the corresponding parameters in the two materials. We found that the tight-binding model with second-neighbor interaction sometimes give rise to spurious interface states if the second-neighbor-interaction parameters for the two materials differ too much. Therefore it is essential to choose the second-neighbor parameters carefully for the two materials in order to avoid the appearance of spurious interface states.

### III. ELECTRONIC STRUCTURES OF GaAs/AlAs SUPERLATTICES

We have calculated the variations of energy bands of  $(\text{GaAs})_M(\text{AlAs})_N$  superlattices with monolayer number  $M$  and  $N$ , applied electric field  $F$ , and parallel wave vector  $k_x$ . We found that the  $\Gamma$ - $X$  crossover can occur against all these parameters. The valence-band offset  $\Delta E_v$  is chosen to be 0.538 eV, so the  $\Gamma$ - $X$  separation in a  $(\text{GaAs})_{12}(\text{AlAs})_{28}$  superlattice agrees with the photoluminescence measurements.<sup>5</sup> This is about 34% of the band-gap difference between AlAs and GaAs, also in agreement with the experimental results of Ref. 34.

Figures 4 and 5 show the variations of electronic states at  $k_{\parallel}=0$  with the number of monolayers of GaAs ( $M$ ) in  $(\text{GaAs})_M(\text{AlAs})_6$  and  $(\text{GaAs})_M(\text{AlAs})_M$  superlattices. In the first case the  $X$  level is basically unchanged due to the constant AlAs thickness. In the second case both the  $\Gamma$  and  $X$  levels descend with increasing  $M$ . The  $\Gamma$  and  $X$  levels cross at  $M=8$  (or 9) and  $M=12$  for the two cases, respectively. The number of GaAs monolayers,  $M=12$ , at which the  $\Gamma$  and  $X$  levels cross, is in agreement with recent experimental results.<sup>6,7</sup>

Figure 6 shows the lowest  $\Gamma$ - and  $X$ -like energy levels of  $(\text{GaAs})_{12}(\text{AlAs})_{12}$  and  $(\text{GaAs})_{13}(\text{AlAs})_{13}$  superlattices as functions of  $k_x$ . Because of the difference in the effective masses between the GaAs  $\Gamma$  band and the AlAs  $X$  band, the  $\Gamma$  and  $X$  energy levels cross at  $k_x=0.015$  and  $0.025(2\pi/a)$  for the two superlattices, respectively. All the levels in Figs. 4-6 are identified by calculating the wave functions and the optical matrix elements between the conduction- and valence-band states. It is noticed that for the  $(\text{GaAs})_{12}(\text{AlAs})_{12}$  superlattice the  $\Gamma$  and  $X$  energy levels cross without interaction, but for the  $(\text{GaAs})_{13}(\text{AlAs})_{13}$  superlattice the  $\Gamma$  and  $X$  levels are mixed when they are close in energy. This can be understood by symmetry arguments, as was first pointed out in

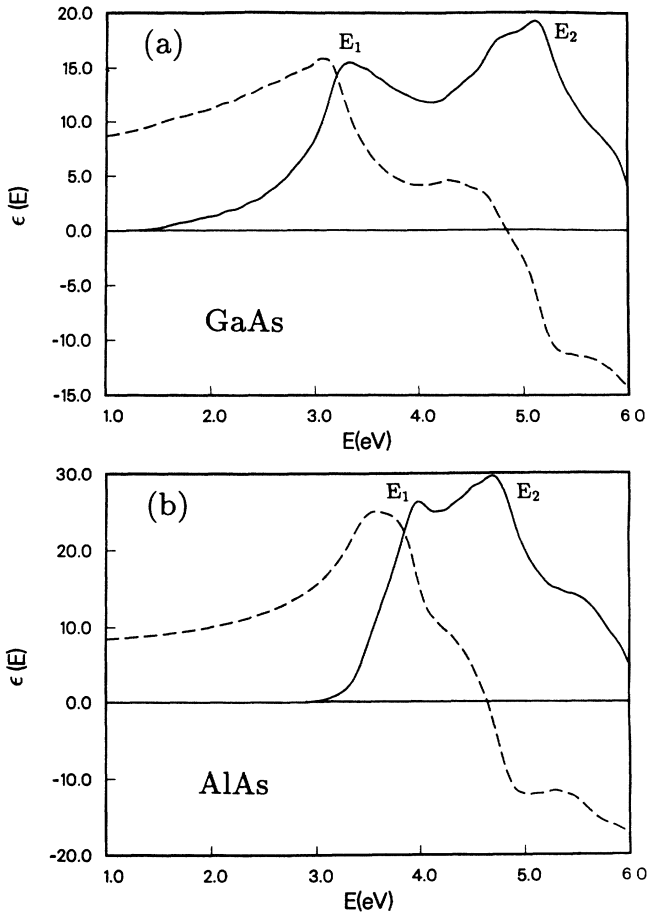


FIG. 3. Dielectric function of (a) GaAs and (b) AlAs. Solid line: imaginary part,  $\epsilon_2(E)$ . Dashed line: real part,  $\epsilon_1(E)$ .

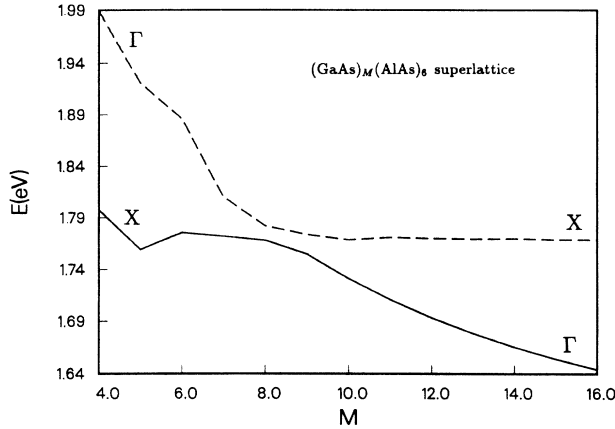


FIG. 4. Lowest two conduction-band energy levels of  $(\text{GaAs})_M(\text{AlAs})_6$  superlattices as functions of  $M$ .

Ref. 19. Since the superlattice has reflection symmetry with respect to the plane through the center of either the GaAs or AlAs layers, only states with the same overall parity can be coupled. The parities of the  $\Gamma$ -valley states are just those for the associated envelope functions. On the other hand, the parities of  $X$ -valley states depend on whether the superlattice contains an even and odd number of monolayers in the AlAs layer ( $N$ ). In the one-band Wannier model<sup>19</sup> the  $X$ -valley states at  $\mathbf{k}=\mathbf{0}$  can be written as

$$|\psi\rangle = \sum_{R_z} F(R_z) e^{ik_0 R_z} |R_z\rangle, \quad (10)$$

where  $F(R_z)$  is an envelope function similar to that obtained in a "particle-in-a-box" model,  $k_0=2\pi/a$ , and  $|R_z\rangle$  denotes the sum of all Wannier orbitals located in the plane at  $z=R_z$ .  $R_z$  is measured with respect to the center of the AlAs layer. The phase factor  $e^{ik_0 R_z}$  has an important effect on the parity of the state. For odd  $N$  the

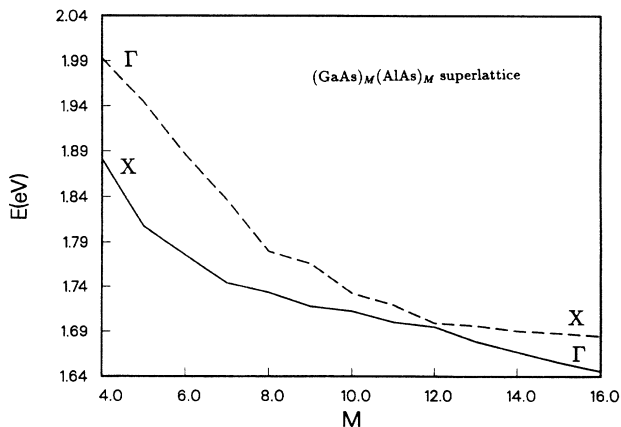


FIG. 5. Lowest two conduction-band energy levels of  $(\text{GaAs})_M(\text{AlAs})_M$  superlattices as functions of  $M$ .

center of the AlAs layer coincides with one Wannier site, and we have  $e^{ik_0 R_z} = \cos(k_0 R_z)$ , since  $\sin(k_0 R_z) = 0$ . So, the overall parity is the same as the parity of the envelope function. For even  $N$ , the center of the AlAs layer is in the middle between two Wannier sites, and we have  $e^{ik_0 R_z} = i \sin(k_0 R_z)$ . So, the overall parity is opposite to the envelope function. In the tight-binding model the argument is similar, but the roles of even and odd numbers of monolayers in the AlAs layer may be different, depending on the character of the  $X$  states. In the tight-binding model, the AlAs  $X$  states can be written as

$$|\psi\rangle = \sum_{\alpha, R_z, i} F_\alpha(R_z + \tau_i) e^{ik_0(R_z + \tau_i)} |\alpha, R_z + \tau_i\rangle, \quad (11)$$

where  $\alpha$  labels the orbital type ( $s, x, y, z$ ),  $i$  labels the atomic species (anion or cation),  $\tau_i=0$  for anion and  $a/4$  for cation,  $F_\alpha$  is the  $\alpha$ -component envelope function, and  $|\alpha, R_z + \tau_i\rangle$  denotes an atomic orbital of type  $\alpha$  located at atomic site  $R_z + \tau_i$ . In the present tight-binding model, the lowest conduction state at  $\mathbf{k}=(0,0,1)(2\pi/a)$  ( $X$  point) consists of a cation  $s$ -like component and an anion  $z$ -like component. With respect to a fixed origin (taken as the center of the AlAs layer), the phase factors  $e^{ik_0(R_z + \tau_i)}$  for anion and cation components have opposite parity, because the phase shift  $k_0\tau_i=0$  and  $\pi/2$  for cation and anion, respectively. The  $s$  and  $z$  orbitals also have oppo-

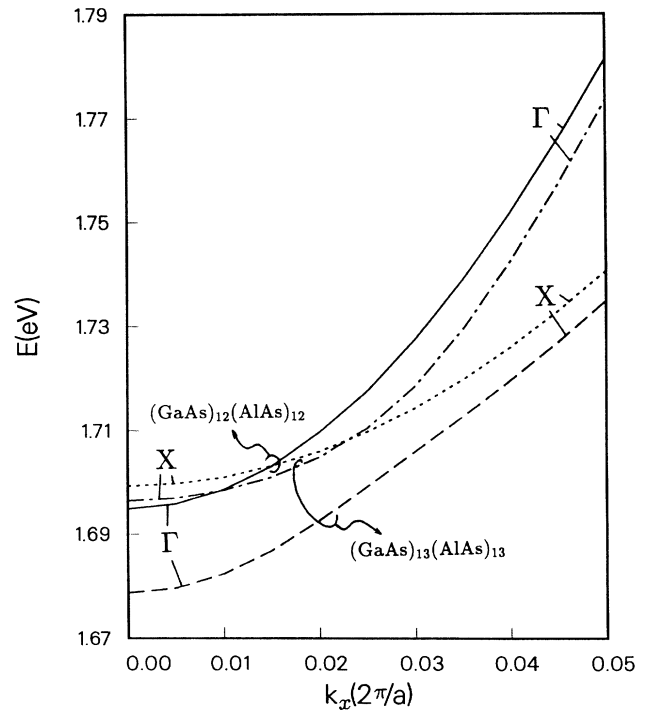


FIG. 6. Lowest two conduction-band energy levels of  $(\text{GaAs})_{12}(\text{AlAs})_{12}$  (solid and dotted curves) and  $(\text{GaAs})_{13}(\text{AlAs})_{13}$  superlattices (dashed-dotted and dashed curves) as functions of the wave vector in the  $x$  direction,  $k_x$ .

site parity. So, the overall parities from the anion and cation contributions are the same. Since the  $\Gamma$  states are predominantly  $s$ -like, it suffices to consider only the  $s$ -like component (therefore, the cation component) in figuring out the  $\Gamma$ - $X$  mixing effect. For odd (even)  $N$  the center of the AlAs layer coincides with one cation (anion) site, and the overall parity is identical (opposite) to that of the cation  $s$ -like envelope function. Thus, the  $\Gamma$ - $X$  mixing only occurs for odd  $N$ , as is predicted in the Wannier model. It should be noted that a different choice of tight-binding parameters (such as in Ref. 17) can lead to the opposite conclusion. Since the tight-binding parameters are not unique, one can obtain an "equally" good fit to the EPM band structure, but with different characters in the states at  $X$ . Thus, in a different tight-binding model the lowest conduction-band state at  $X$  may consist of an anion  $s$ -like component and a cation  $z$ -like component (due to a switch of roles of the fifth and sixth conduction bands at  $X$ ), and the prediction regarding even or odd  $N$  for the  $\Gamma$ - $X$  mixing to occur would be reversed.

Thus, the disagreement or agreement between the predictions of the tight-binding model and the Wannier model is determined by whether the  $s$ -like component of the lowest  $X$  state in AlAs is nonvanishing on the anion or cation. In Ref. 17 Lu and Sham also discussed the effect of general crystalline symmetry of the superlattice on the other valley-mixing effects. They showed that some superlattice electronic properties depend on whether the total number of diatomic layers ( $M+N$ ) is even or

odd, since the superlattice has different crystalline symmetry for even or odd ( $M+N$ ). It should be made clear that the  $\Gamma$ - $X_z$  mixing discussed here depends only on whether the number of AlAs diatomic layers ( $N$ ) is even or odd, independent of the total crystalline symmetry. For example, as shown in Fig. 6 both  $(\text{GaAs})_{12}(\text{AlAs})_{12}$  and  $(\text{GaAs})_{13}(\text{AlAs})_{13}$  superlattices have the same crystalline symmetry, but different  $\Gamma$ - $X_z$ -mixing behavior.

Figure 7 shows the lowest two conduction-band energy levels (measured with respect to the highest valence-subband level) as functions of the applied electric field  $F$  for a  $(\text{GaAs})_{12}(\text{AlAs})_{28}$  superlattice. The corresponding experimental results of Ref. 5 are also shown (solid circles) for comparison. In this calculation we assumed that the potential caused by the electric field is periodic with the same period as the superlattice. From Fig. 7 we see that the  $\Gamma$  level does not change appreciably with the applied electric field, i.e., the Stark effect is not apparent for the short-period superlattice. The  $X$  levels rise as the applied field increases because of the potential difference between the center of two adjacent layers. The variation of the  $\Gamma$  and  $X$  levels with the applied electric field is in good agreement with the experimental results. The  $\Gamma$  and  $X$  energy levels anticross at  $F = 4.5 \times 10^4$  V/cm, as does the experimental value. The energy splitting at the crossing field is about 2 meV, also the same as the experimental value of 2 meV. Note that the anticrossing behavior is seen even though the number of AlAs layers is even. This is because the presence of the electric field destroys the reflection symmetry. The numbers in parentheses along the energy axis denote the experimental transition energies. The theoretical values appear to be higher than the experimental values by about 30 meV. Part of the difference is due to the exciton binding energy, which is ignored in the calculation.

Semiconductor superlattices have also been grown along the [111] direction and they have shown some interesting properties—for example, the strain-induced internal electric field effect (piezoelectric effect),<sup>35,36</sup>

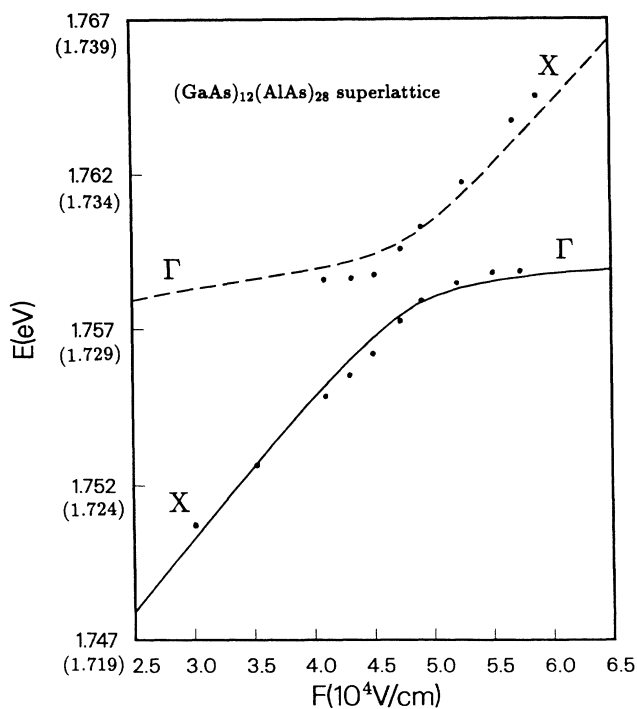


FIG. 7. Lowest two conduction-band energy levels of a  $(\text{GaAs})_{12}(\text{AlAs})_{28}$  superlattice as functions of the applied electric field  $F$ . Solid and dashed curves: theory. Solid circles: data from Ref. 5.

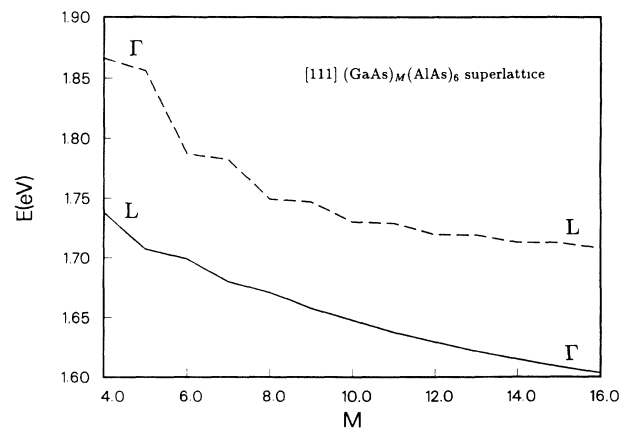


FIG. 8. lowest two conduction-band energy levels of [111]-grown  $(\text{GaAs})_M(\text{AlAs})_6$  superlattices as functions of  $M$ .

enhanced photoluminescence intensity, and reduced threshold current density for laser structures,<sup>37</sup> etc. The electronic energy levels as functions of the number of GaAs monolayers for  $(\text{GaAs})_M(\text{AlAs})_6$  superlattices are shown in Fig. 8. Instead of  $\Gamma$ - $X$  crossover, we found a  $\Gamma$ - $L$  crossover in this case. The  $\Gamma$ - $L$  crossover is due to the different effective masses of the two bands. It differs from the  $\Gamma$ - $X$  crossover in that both the  $\Gamma$  and  $L$  states are localized in the same GaAs layer, i.e., no spatial separation. Comparing Fig. 8 with Fig. 4, we see that the interaction caused by the  $\Gamma$ - $L$  mixing is apparently larger than that of the  $\Gamma$ - $X$  mixing. The  $\Gamma$ - $L$  crossover occurs near  $M=6$ , where the mixing between  $\Gamma$ - and  $L$ -like states is strongest, resulting in comparable optical matrix elements for transitions from the first heavy-hole state (HH1) to the two lowest conduction-band states. The  $L$ -like energy level as a function of the number of GaAs layers ( $M$ ) displays an odd-even oscillatory behavior, with lower values at even numbers of  $M$ . This indicates that the  $\Gamma$ - $L$  mixing is also sensitive to whether  $M$  is even or odd. Unlike the [001] case the [111]-grown superlattice does not possess reflection symmetry with respect to any plane parallel to the interface. However, if the  $s$ -like component of the lowest conduction-band state at  $L$  is appreciable only on a cation (or an anion), one can ignore the presence of the other atomic species, and the argument for the  $\Gamma$ - $X$  mixing discussed above can still be used. For the present tight-binding model the lowest conduction-band state at  $L$  consists of about 44% cation  $s$  character and 21% anion  $s$  character (the rest being  $p$ -like). Using the argument given for the  $\Gamma$ - $X$  mixing, we then predict that the  $\Gamma$ - $L$  mixing is stronger for odd  $M$  than for even  $M$ . For odd  $M$  the  $\Gamma$  and  $L$  levels have the same symmetry (as far as the cations are concerned), and they repel each other as a result of the interaction. The hole-subband structure has been discussed in Refs. 36 and 38. In Table IV we give the squared optical matrix elements from the first heavy- and light-hole states HH1 and LH1 to the lowest two electronic levels  $E1$  and  $E2$  (at  $\mathbf{k}_{\parallel}=0$ ) for  $(\text{GaAs})_M(\text{AlAs})_6$  [111] superlattices. From Table IV we see that, when  $M=4$ , the lowest-energy level is  $L$ -like with small transition probabilities, and the second level is  $\Gamma$ -like. When  $M \geq 7$  the lowest-energy levels are  $\Gamma$ -like with large transition probabilities, and the second levels are  $L$ -like. At  $M=6$  there is apparent  $\Gamma$ - $L$  mixing, resulting in comparable transition probabilities for the two levels.

#### IV. DIELECTRIC FUNCTIONS OF SUPERLATTICES

In the calculation of the dielectric function of superlattices, one needs to perform summations over the conduction- and valence-subband indices and wave vectors in the surface Brillouin zone [see Eqs. (5) and (6)]. Both the pseudopotential and effective-mass methods are not suitable for this kind of calculation, because the former needs too much computation time, and the latter can only get reliable superlattice energies and wave functions around one symmetry point (usually the  $\Gamma$  point). The tight-binding method with properly chosen empirical parameters, which give the correct band structures, is most suitable for calculating the dielectric function of superlattices in the full energy range. In our calculations the integrations in Eqs. (5) and (6) over superlattice wave vectors are replaced by summations over special points in the two-dimensional Brillouin zone<sup>39</sup> ( $k_x, k_y$ ) and in the one-dimensional Brillouin zone ( $k_z$ ). We took 36 special points in the  $\frac{1}{8}$  two-dimensional Brillouin zone  $[(\frac{1}{16}, 0), \dots]$  and two special points in the  $\frac{1}{2}$  one-dimensional Brillouin zone  $[\frac{1}{4}, \frac{3}{4}]$ . The contribution from each special point is broadened, with half-width  $\Gamma$  taken to be 0.1 eV. The  $\frac{1}{16}$  segments of the two-dimensional Brillouin zone for the (001) superlattice is depicted in Fig. 9. The solid circles denote the special points used in the summation. The segment is divided into four regions (labeled 1–4), so that separate contributions from these four regions can be identified.

Figure 10 shows the imaginary part of the dielectric function  $\epsilon_2(E)$  of a  $(\text{GaAs})_6(\text{AlAs})_6$  superlattice (solid curve). Contributions from various portions of the Brillouin zone are also displayed, which are marked 1–4, corresponding to the four regions shown in Fig. 9. Comparing this figure with Fig. 3, we find that  $\epsilon_2(E)$  of the superlattice is apparently different from  $\epsilon_2(E)$  of either GaAs or AlAs. The lower-energy tail near the band gap shifts from the bulk GaAs energy gap ( $\approx 1.5$  eV) to near 2 eV due to the quantization effect and it is predominantly derived from region 1 (around the zone center). The  $E_1$  peak of bulk GaAs, which is derived mainly from region 3 (near the  $L$  point), turns into a weak shoulder and moves to higher energy (near 3.5 eV) in the superlattice spectrum. A hump appears in the superlattice  $\epsilon_2$  spectrum near 4.0 eV, which is mainly contributed from regions 3 and 4, sitting on the broad background contribut-

TABLE IV. Squared optical matrix elements for  $(\text{GaAs})_M(\text{AlAs})_6$  [111]-grown superlattices (in eV) from first heavy-hole (HH1) and light-hole (LH1) states to the lowest two electronic states ( $E1$  and  $E2$ ).  $P_z$  and  $P_{\parallel}$  are the components of  $\mathbf{P}$  [Eq. (7)] in the grown direction and the direction parallel to the interface, respectively.

|                        | $M$      |          |          |          |          |          |          |          |          |          |
|------------------------|----------|----------|----------|----------|----------|----------|----------|----------|----------|----------|
|                        | 4<br>HH1 | 4<br>LH1 | 5<br>HH1 | 5<br>LH1 | 6<br>HH1 | 6<br>LH1 | 7<br>HH1 | 7<br>LH1 | 8<br>HH1 | 8<br>LH1 |
| $ P_{\parallel} ^2 E1$ | 1.477    | 1.003    | 2.485    | 1.629    | 3.095    | 1.959    | 3.942    | 2.397    | 4.883    | 2.850    |
| $ P_z ^2 E1$           | 0.010    | 1.260    | 0.015    | 1.882    | 0.018    | 2.464    | 0.022    | 3.177    | 0.027    | 4.082    |
| $ P_{\parallel} ^2 E2$ | 4.350    | 2.801    | 3.777    | 2.395    | 3.169    | 1.946    | 2.763    | 1.623    | 1.874    | 1.059    |
| $ P_z ^2 E2$           | 0.031    | 2.190    | 0.027    | 2.061    | 0.020    | 1.751    | 0.018    | 1.637    | 0.011    | 1.090    |

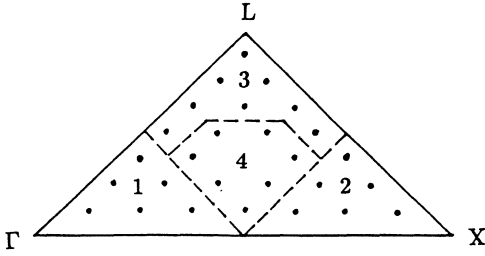


FIG. 9. Two-dimensional Brillouin zone for (001) superlattices divided into four regions (labeled 1-4).

ed from region 1. This structure is related to the AlAs  $E_1$  peak. Another strong peak appears near 4.7 eV, which is mainly derived from region 2 (near the X point). The peak position coincides with the  $E_2$  peak of AlAs. For comparison we also calculate the average of  $\epsilon_2(E)$  of bulk GaAs and AlAs by treating them separately as a superlattice with a period of 12 monolayers. The results are also shown in Fig. 10 (dotted curve). We see that  $\epsilon_2(E)$  of the superlattice is close to the average  $\epsilon_2(E)$  of GaAs and AlAs, but with some discernibly different features. The structures marked  $E_1$  and  $E_2$  are derived from GaAs, and those marked  $\tilde{E}_1$  and  $\tilde{E}_2$  are from AlAs. The main difference between the average spectrum and the superlattice spectrum is that the structure  $\tilde{E}_1$  becomes less pronounced and shifts toward higher energy in the superlattice spectrum.

To understand the variation of  $\epsilon_2(E)$  with the monolayer number  $M$  for  $(\text{GaAs})_M(\text{AlAs})_M$  superlattices, we calculated  $\epsilon_2(E)$  of  $(\text{GaAs})_4(\text{AlAs})_4$  and  $(\text{GaAs})_{10}(\text{AlAs})_{10}$  superlattices, and compare them with the previous results of the  $(\text{GaAs})_6(\text{AlAs})_6$  superlattice and the GaAs-AlAs average. The comparison is shown in Fig. 11. We see

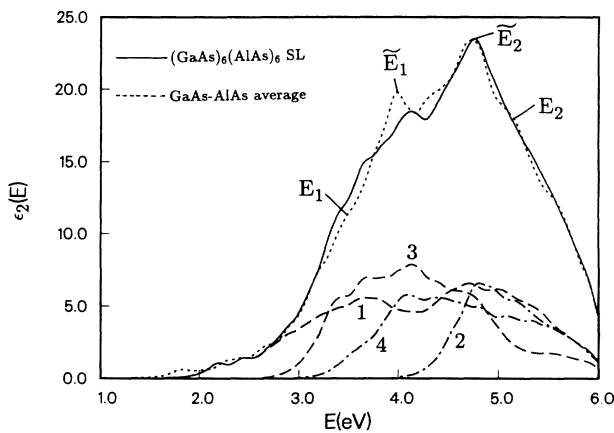


FIG. 10. Imaginary part of the dielectric function  $\epsilon_2(E)$  for a  $(\text{GaAs})_6(\text{AlAs})_6$  superlattice (solid curve) and the average  $\epsilon_2(E)$  of bulk GaAs and AlAs (dotted curve). Curves 1-4 are various contributions for the superlattice from regions 1-4 defined in Fig. 9.

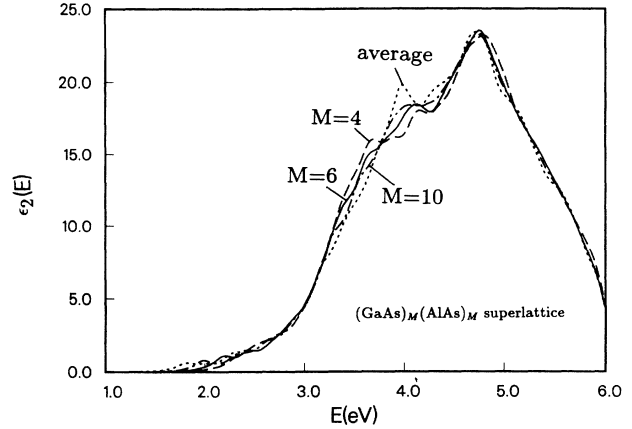


FIG. 11. Imaginary part of the dielectric function,  $\epsilon_2(E)$ , of  $(\text{GaAs})_M(\text{AlAs})_M$  superlattices:  $M=4$  (dashed curve),  $M=6$  (solid curve), and  $M=10$  (dashed-dotted curve). The average  $\epsilon_2(E)$  of bulk GaAs and AlAs (dotted curve) is also included for comparison.

that for  $(\text{GaAs})_4(\text{AlAs})_4$  superlattice there are three peaks in the  $\epsilon_2$  spectrum. The first two peaks are derived from the  $E_1$  peak of bulk GaAs (shifted upward in energy due to confinement and AlAs). The third is derived from the  $E_2$  peak of AlAs. The  $\epsilon_2(E)$  spectrum of the  $(\text{GaAs})_{10}(\text{AlAs})_{10}$  superlattice is very close to that of the GaAs-AlAs average. We thus conclude that for  $(\text{GaAs})_M(\text{AlAs})_M$  superlattices with large  $M$  ( $\geq 10$ ), the global optical properties can be approximately obtained by simply taking the average of those for the constituent materials.

Figure 12 shows the  $\epsilon_1(E)$  of  $(\text{GaAs})_M(\text{AlAs})_M$  superlattices ( $M=4,6,10$ ) and the GaAs-AlAs average. Again, we see the similarity between the superlattice spectrum

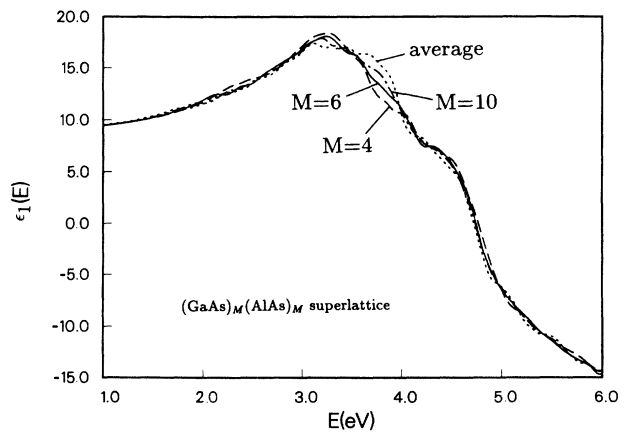


FIG. 12. Real part of the dielectric function,  $\epsilon_1(E)$ , of  $(\text{GaAs})_M(\text{AlAs})_M$  superlattices:  $M=4$  (dashed curve),  $M=6$  (solid curve), and  $M=10$  (dashed-dotted curve). The average  $\epsilon_1(E)$  of bulk GaAs and AlAs (dotted curve) is also included for comparison.

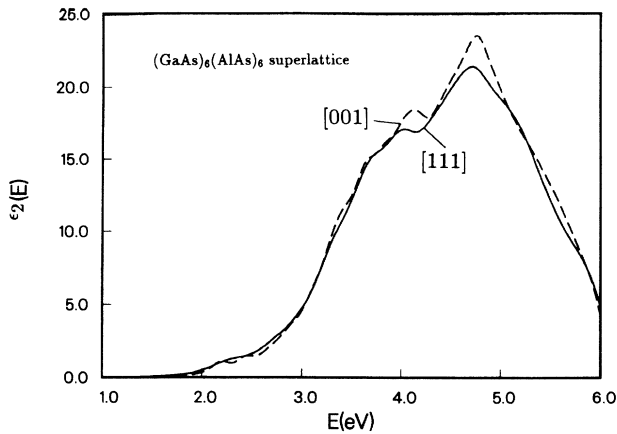


FIG. 13.  $\epsilon_2(E)$  for the  $(\text{GaAs})_6(\text{AlAs})_6$  superlattice grown in the [111] (solid curve) and [001] directions (dashed curve).

and the average GaAs-AlAs spectrum, especially for superlattices with large  $M$ .

Garriga *et al.* have reported ellipsometric measurements of the dielectric functions of short-period GaAs-AlAs superlattices.<sup>24</sup> They found that for ultrathin-layer superlattices [e.g.,  $(\text{GaAs})_1(\text{AlAs})_1$  and  $(\text{GaAs})_3(\text{AlAs})_3$ ], the measured  $\epsilon_2(E)$  spectra contain two principal peaks associated with the  $\tilde{E}_1$  and  $\tilde{E}_0 + \tilde{E}_2$  transitions, respectively. The peak positions are approximately given by the average of the corresponding GaAs and AlAs values. Our theoretical predictions are consistent with these measurements. However, the  $\tilde{E}_1$  peak predicted in our theory is consistently weaker than that observed experimentally. The main reason for this is the neglect of the excitonic effect in our calculations. For wider-layer superlattices [e.g.,  $(\text{GaAs})_{15}(\text{AlAs})_{15}$ ], some additional structures below the  $\tilde{E}_1$  peak are observed experimentally. These structures are exciton resonances associated with the confined subbands with wave vectors near the  $L$  point. Since we did not include the excitonic effect, these structures are absent in our calculated spectra.

We have also calculated  $\epsilon_2(E)$  of [111]-grown superlattices, taking 18 special points in the  $\frac{1}{2}$  hexagonal two-dimensional Brillouin zone,<sup>39</sup> and using 0.15 eV for the half-width  $\Gamma$ . The result for a  $(\text{GaAs})_6(\text{AlAs})_6$  [111]-grown superlattice is shown in Fig. 13, compared with

that of the [100]-grown  $(\text{GaAs})_6(\text{AlAs})_6$  superlattice. The  $\epsilon_2(E)$ 's of the two oriented superlattices are similar.

## V. SUMMARY

In this paper we used a second-neighbor tight-binding model to study the electronic structures and optical properties (dielectric functions) of short-period superlattices. We found that it is essential to choose suitable second-neighbor-interaction parameters for the constituent materials to get correct band structures of the superlattice. For bulk materials, we obtained energy bands and dielectric functions in good agreement with the experimental results. For superlattices, we calculated the  $\Gamma$ - and  $X$ -like energy levels as functions of the number of GaAs monolayers, the applied electric field, and the parallel wave vector. The results for the  $\Gamma$ - $X$  crossover are in agreement with the available data. We also calculated the [111]-grown GaAs/AlAs superlattices and predicted the behavior of  $\Gamma$ - $L$  crossover. We found that the mixing between  $\Gamma$ - and  $L$ -like electronic states is much stronger than the corresponding  $\Gamma$ - $X$  mixing in the [001]-grown GaAs/AlAs superlattices. The optical matrix elements  $|P_{\parallel}|^2$  and  $|P_z|^2$  are nearly the same for heavy-hole- or light-hole-to-conduction-band transitions as a result of strong mixing.

We calculated the real and imaginary parts of the dielectric function of short-period superlattices in the full energy range. It is found that the dielectric functions of the  $(\text{GaAs})_M(\text{AlAs})_M$  superlattices are apparently different from that of bulk GaAs and AlAs. When the number of monolayers  $M$  of the  $(\text{GaAs})_M(\text{AlAs})_M$  superlattices increases, the  $\epsilon_2(E)$  [also  $\epsilon_1(E)$ ] gradually approach the average dielectric functions of bulk GaAs and AlAs. We found that the  $\epsilon_2(E)$  for [111]-grown superlattices are similar to that for [001]-grown superlattices. It should be noted that the exciton effect has not been taken into account in this paper, which may be necessary for comparing the theoretical results with data.

## ACKNOWLEDGMENTS

This work was supported in part by the U.S. Office of Naval Research (ONR) under Contract N00014-89-J-1157. The use of the computing facilities of the University of Illinois Materials Research Laboratory, supported by the U.S. National Science Foundation (NSF) under Grant No. NSF-DMR-86-12860, is acknowledged.

\*Permanent address: Institute of Semiconductors, Chinese Academy of Sciences, P.O. Box 912, Beijing 100083, China.

<sup>1</sup>E. Finkman, M. D. Sturge, and M. C. Tamargo, *Appl. Phys. Lett.* **49**, 1299 (1986).

<sup>2</sup>J. Nagle, M. Garriga, W. Stolz, T. Isu, and K. Ploog, *J. Phys. (Paris) Colloq.* **48**, C5-495 (1987).

<sup>3</sup>K. J. Moore, P. Dawson, and C. T. Foxon, *J. Phys. (Paris) Colloq.* **48**, C5-525 (1987).

<sup>4</sup>G. Danan, B. Etienne, F. Mollet, and R. Planel, *Appl. Phys. Lett.* **51**, 1605 (1987).

<sup>5</sup>M. H. Meynadier, R. E. Nahory, J. M. Worlock, M. C. Tamargo, J. L. de Miguel, and M. D. Sturge, *Phys. Rev. Lett.* **60**,

1338 (1988).

<sup>6</sup>G. H. Li, D. S. Jiang, H. X. Han, Z. P. Wang, and K. Ploog, *Phys. Rev. B* **40**, 10430 (1989).

<sup>7</sup>R. Cingolani, L. Tapfer, Y. H. Zhang, R. Muralidharan, and K. Ploog, *Phys. Rev. B* **40**, 6101 (1989).

<sup>8</sup>H. Fujimoto, C. Hamaguchi, T. Nakazawa, K. Imanishi, K. Taniguchi, and S. Sasa (unpublished).

<sup>9</sup>Ed Caruthers and P. J. Lin-Chung, *Phys. Rev. B* **17**, 2705 (1978).

<sup>10</sup>W. E. Pickett, S. G. Louie, and M. L. Cohen, *Phys. Rev. B* **17**, 815 (1978).

<sup>11</sup>W. Andeoni and R. Car, *Phys. Rev. B* **21**, 3334 (1980).

- <sup>12</sup>T. Nakayama and H. Kamimura, *J. Phys. Soc. Jpn.* **54**, 4726 (1985).
- <sup>13</sup>M. A. Gell and M. Jaros, *Superlatt. Microstruct.* **3**, 121 (1987).
- <sup>14</sup>J. B. Xia, *Phys. Rev. B* **38**, 8358 (1988).
- <sup>15</sup>J. Ihm, *Appl. Phys. Lett.* **50**, 1068 (1987).
- <sup>16</sup>L. Brey and C. Tejedor, *Phys. Rev. B* **35**, 9112 (1987).
- <sup>17</sup>Y. T. Lu and L. J. Sham, *Phys. Rev. B* **40**, 5567 (1989).
- <sup>18</sup>H. Fujimoto, C. Hamaguchi, T. Nakazawa, K. Tauguchi, and K. Imanishi, *J. Phys. Soc. Jpn.* (to be published).
- <sup>19</sup>D. Z.-Y. Ting and Y. C. Chang, *Phys. Rev. B* **36**, 4357 (1987).
- <sup>20</sup>P. Lantenschlager, M. Garriga, S. Logothetidis, and M. Cardona, *Phys. Rev. B* **36**, 9174 (1987), and references therein.
- <sup>21</sup>T. P. Walter and M. L. Cohen, *Phys. Rev.* **183**, 763 (1969).
- <sup>22</sup>C. S. Wang and B. M. Klein, *Phys. Rev. B* **24**, 3417 (1981).
- <sup>23</sup>K. B. Kahen and J. P. Leburton, *Phys. Rev. B* **32**, 5177 (1985).
- <sup>24</sup>M. Garriga, M. Cardona, N. E. Christensen, P. Lantenschlager, T. Isu, and K. Ploog, *Phys. Rev. B* **36**, 3254 (1987).
- <sup>25</sup>H. Yamamoto, H. Asada, and Y. Suematsu, *Electron. Lett.* **21**, 579 (1985).
- <sup>26</sup>K. B. Kahen and J. P. Leburton, *Phys. Rev. B* **33**, 5465 (1986).
- <sup>27</sup>Y. C. Chang, J. N. Schulman, and U. Efron, *J. Appl. Phys.* **62**, 4533 (1987).
- <sup>28</sup>Y. C. Chang and J. N. Schulman, *Phys. Rev. B* **31**, 2069 (1985).
- <sup>29</sup>Y. C. Chang and D. E. Aspnes, *Phys. Rev. B* **41**, 12 002 (1990).
- <sup>30</sup>P. Vogl, H. P. Hjalmarson, and J. D. Dow, *J. Phys. Chem. Solids* **44**, 365 (1983).
- <sup>31</sup>D. J. Chadi and M. L. Cohen, *Phys. Rev. B* **8**, 5747 (1973).
- <sup>32</sup>M. Garriga, P. Lautenschlager, M. Cardona, and K. Ploog, *Solid State Commun.* **61**, 157 (1987).
- <sup>33</sup>W. Hanke and L. J. Sham, *Phys. Rev. B* **21**, 4656 (1980).
- <sup>34</sup>D. J. Wolford, T. F. Kuech, J. A. Bradley, M. A. Gell, D. Ninni, and M. Jaros, *J. Vac. Sci. Technol. B* **4**, 1043 (1986).
- <sup>35</sup>D. L. Smith and C. Mailhot, *Phys. Rev. Lett.* **58**, 1264 (1987).
- <sup>36</sup>C. Mailhot and D. L. Smith, *Phys. Rev. B* **35**, 1242 (1987).
- <sup>37</sup>T. Hayakawa, K. Takahasi, M. Kondo, T. Suyama, S. Yamamoto, and T. Hijikata, *Phys. Rev. Lett.* **60**, 349 (1988).
- <sup>38</sup>M. P. Houng, Y. C. Chang, and W. I. Wang, *J. Appl. Phys.* **64**, 4609 (1988).
- <sup>39</sup>S. L. Cunningham, *Phys. Rev. B* **18**, 4988 (1974).